Imaging the water snowline in a protostellar envelope with $H^{13}CO^{+}$★

Merel L.R. van 't Hoff[1], Magnus V. Persson[2], Daniel Harsono[1], Vianney Taquet[1,3], Jes K. Jørgensen[4], Ruud Visser[5], Edwin A. Bergin[6], and Ewine F. van Dishoeck[1,7]

背景：スノーラインの位置を観測的に制限することは、惑星形成メカニズムの解明に不可欠
最も重要な水のスノーラインは、原始惑星円盤での直接観測することがとても難しい

目的：HCO^{+}は水のスノーラインの良いトレーサーなのか。
低質量星NGC1333-IRAAS2Aのエンベロープに対し、光学的に薄い$H^{13}CO^{+}$でマップピング。
$H_2{}^{18}O$観測結果との比較で、本当にこれがよいトレーサーかどうかわかる。

観測：NOrthern Extended Millimeter Array (NOEMA) @ ~0.9'' 分解能
$H^{13}CO^{+}$ J=3-2 @ 260.255 GHz

Table 1. Overview of the molecular line observations toward IRAS2A.

Transition	Frequency (GHz)	E_{up}/k (K)	Beam ($''$)	Δv^a (km s^{-1})
$H^{13}CO^{+}$ $J = 3-2$	260.255	25	0.93×0.68	0.09
$H_2^{18}O$ $3_{1,3}-2_{2,0}$	203.408	204	0.87×0.72	0.115
DCO^{+} $J = 2-1$	144.068	10	2.1×1.7	4.06

Notes. [(a)] Velocity resolution.

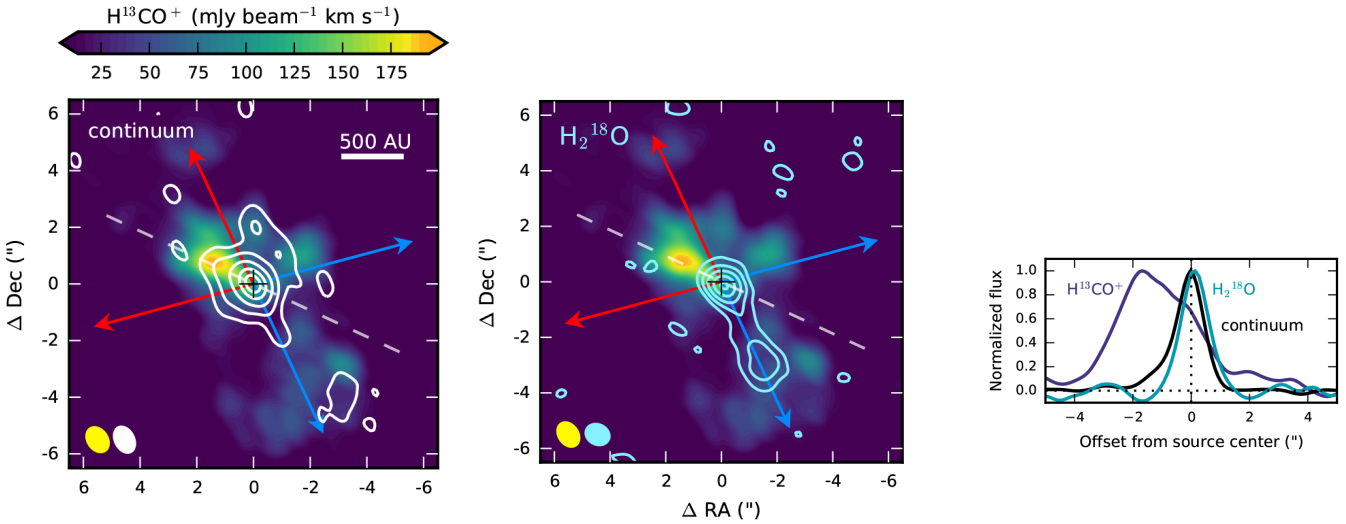

Fig. 2. Integrated intensity map for the $H^{13}CO^{+}$ $J = 3-2$ transition (color scale) toward IRAS2A, with the 1.2 mm continuum overlaid in white contours (*top panel*) and the $H_2^{18}O$ $3_{1,3}-2_{2,0}$ transition in blue contours (*middle panel*). The continuum contours are 1.8 (1σ) × [3, 10, 25, 50, 75] mJy beam^{-1}, and the $H_2^{18}O$ contours are 9.8 (1σ) × [3, 8, 15, 25, 35] mJy beam^{-1} km s^{-1}. The beams are depicted in the lower left corners. The position of the continuum peak is marked by a black cross (the close binary is unresolved in these data) and the outflow axes by red and blue arrows. The integrated intensities along the dashed white line are shown in the *bottom panel*, normalized to their maximum value. The zero flux level and source position are marked by dotted lines.

H13CO+のemission peak：　continuum peakの北~2''
一方、$H_2{}^{18}O$はコンパクトなemission

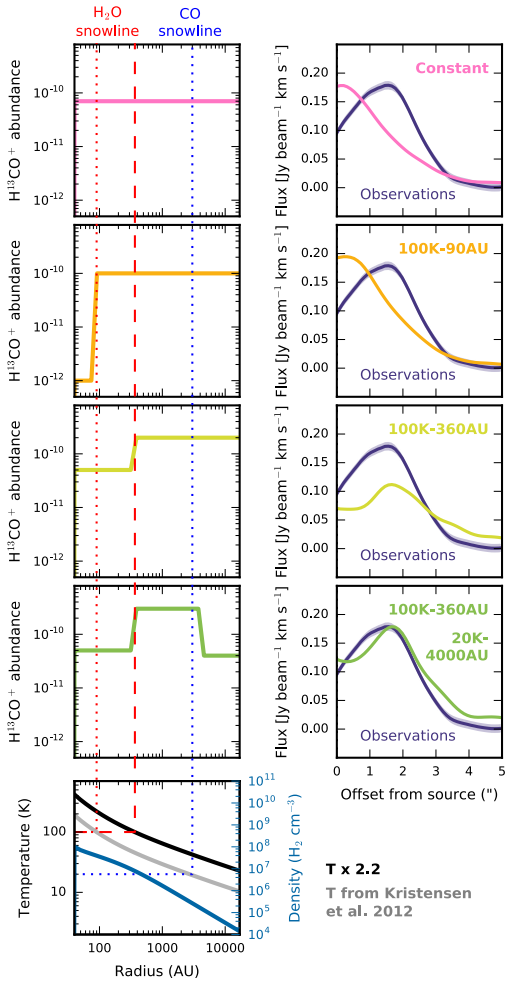

Fig. 5. Different $H^{13}CO^+$ abundance profiles (*left panels*) and the resulting simulated integrated emission along the northeastern part of the radial cut shown in Fig. 2 (*right panels*). The observed emission is shown in purple. The location of the abundance jumps (in Kelvin and AU) is indicated in the top right corners. *Bottom panel:* Temperature (gray) and density (blue) profiles for the IRAS2A envelope from Kristensen et al. (2012) used in the top two models. The location of the H_2O and CO snowlines (at 100 K and 20 K, resp.) are marked by the dotted red and blue lines, respectively. The temperature profile increased by a factor of 2.2, used in the bottom two models, is shown in black. The resulting H_2O snowline is indicated by the dashed red line while the CO snowline now falls outside the adopted radial range. For IRAS2A, 1″ corresponds to ~250 AU.

=> 定量的モデル：　このずれは、360AU以内での$H^{13}CO^+$のabundance の減少で説明できる。

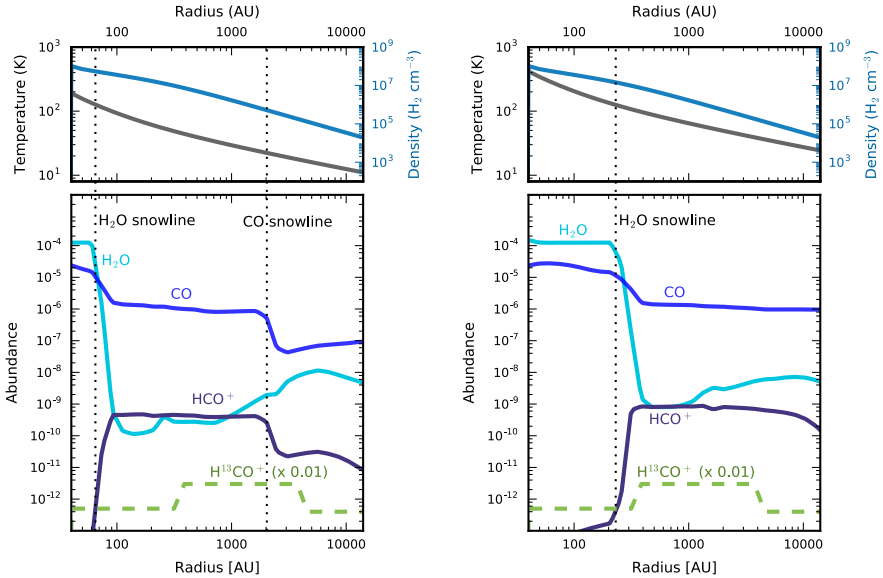

Fig. 6. *Left panels:* Temperature (gray) and density (blue) profiles for the IRAS2A envelope from Kristensen et al. (2012) (*top*), and the corresponding H_2O (light blue), CO (blue) and HCO^+ (purple) abundances predicted by the GRAINOBLE model (*bottom*). The dashed green line shows the empirically inferred abundance profile for $H^{13}CO^+$ (scaled down by a factor 100). *Right panels:* As left panels, but with the temperature increased by a factor 2.2. The vertical dotted lines mark the H_2O and CO snowlines.

水スノーラインの丁度外側で$H^{13}CO^+$が増加：
　化学モデルの予測と一致
　（水スノーラインが225AU付近で、
　　一方$H^{13}CO^+$のabundanceピークは360AUからさらに135AU外側）
　水スノーラインは225AUに置かれる。

　1Dエンベロープの温度構造から予測される距離よりも、かなり遠い

$H^{13}CO^+$と$H_2{}^{18}O$の空間的不一致：
　「$H^{13}CO^+$は水スノーラインのトレーサーとして使える」ことを示す。

The Near-Infrared Outflow and Cavity of the proto-Brown Dwarf Candidate ISO-Oph 200⋆

Whelan, E.T.[1], Riaz, B.[2], and Rouzé, B.[1]

proto-brown dwarf候補天体のNIR観測論文。

天体：ISO-Oph 200（0,06+-0.01 Msun）。SEDからClass Iと考えられている（Evans+09）

観測：integral field spectrograph SINFONIを使ってVLTで観測。

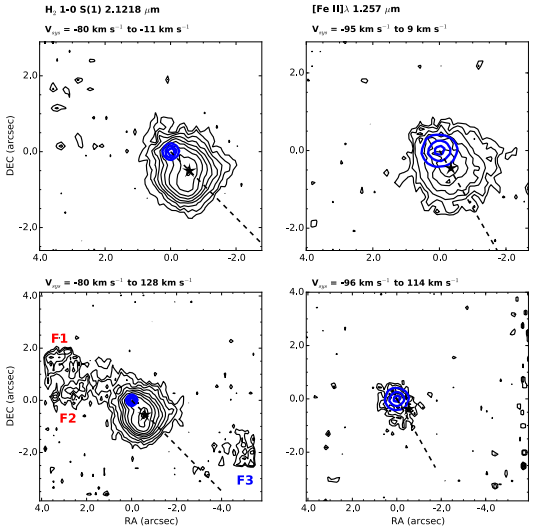

Fig. 2. Continuum subtracted spectro-images of the ISO-Oph 200 outflow in the H_2 1-0 S(1) and [Fe II] 1.257 μm lines. Velocities have been corrected for the systemic velocity of the source. **Top panels:** Here the emission in a mainly blue-shifted velocity range is shown to highlight the blue-shifted jet emission only. Black contours begin at 3σ and increase in multiples of 1.5. $1\sigma = 4.5 \times 10^{-15}$ erg cm^{-2} s^{-1} μm^{-1}. The blue contours show the continuum emission and they correspond to 50%, 75% and 95% of the peak flux of the continuum. The black stars marks the position of the emission peaks and the emission PA is delineated by the dashed line). **Bottom panels:** Here the emission in the velocity ranges -80 km s^{-1} to 128 km s^{-1} (H_2) and -96 km s^{-1} to 114 km s^{-1} ([Fe II]) is shown. This range was chosen to show simultaneously the extended blue and red-shifted low velocity H_2 emission which it is argued traces the cavity. The chosen range also shows that there is no red-shifted counterpart to the blue-shifted jet emission and that the cavity emission is not seen in [FeII]. Contours start at 3σ and increase in multiples of 1.5. $1\sigma = 5 \times 10^{-15}$ erg cm^{-2} s^{-1} μm^{-1}. The continuum emission is plotted in the same way as for the top panels.

コンパクトなblueシフトoutflow：　全てのラインで見えている

速度の遅い（~ +-10km/s）red&blueシフトの広がったemission：
H2のみで見える
方向は、速いコンパクトなemissionとは異なるPAを持っている。

Outflow Feature	V_{sys} (km s^{-1})	Offset ($''$)	PA ($\circ$)
H_2 Jet	-35 ±2	0.″7	230
Fe II Jet	-51 ± 5	0.″5	215
F1	4 ± 3	4.″0	67
F2	10 ± 3	2.″6	80
F3	-14 ± 5	5.″4	248

Table 1. Outflow emission features and corresponding properties. Offsets are with respect to the source position and along the given PA. PAs are measured E of N. It is argued that F1, F2 and F3 form part of a cavity around the jet.

コンパクトemission => jet
広がったH2 emission => cavityをトレース

Sourceの減光量：　Av = 18 mag +- 1 mag
Outflowの減光量：　Av = 9 mag +- 0.4 mag

with color-color diagram (Davis+11)

H2 outflowの温度：　1422 K +- 255 K
[Fe II]の電子密度：　~10000 cm^{-3}

mass outflow rate：
For H2,　　$M = 3.8 \times 10^{-10}\ M_{sun}/yr$
For FeII,　　$M = 1.0 \times 10^{-8}\ M_{sun}/yr$

PaβとBrγ線のLuminosity、
星の質量（0.06 - 0.1 M_{sun}）、
半径（0.9 - 0.5 R_{sun} ）を用いて：
M_{acc} ~ (3-10) x 10^{-8} M_{sun}/yr

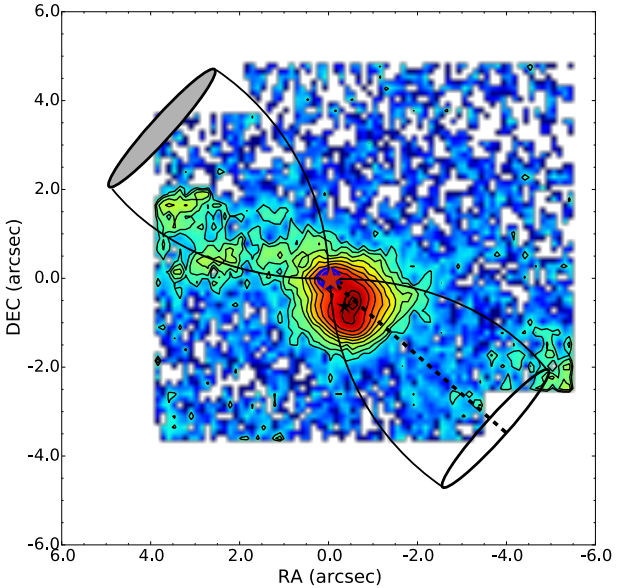

Fig. 3. Colour map of the full H_2 1-0 S(1) emission. The colours are shown to highlight the difference intensity between the H_2 jet emission along a PA of 230° (dashed line) and the extended emission which likely delineates a cavity. A cavity with opening angle 40° is overlain here and well represents the extended fainter emission.

広がったH2 emissionが、H2・[Fe II]の両方で見られるものと違うgeometryを持っている
＝　我々が見ているものはwind-swept cavity

Opening angle ~40° にfittingできる：
Davis+02のClass I天体の値の範囲内

proto-BDのNIR観測は、BD質量天体のjetを調べるには良いツール。
広い角度のwindのようなoutflow成分の証拠を探すことができ、
jetの減光が調べられ、jetの効率が測定できる。
近い将来、JWST/NIRSPECを使ったより高分解能でのjetのcollimationやstructureの観測が可能になる。

Gravity drives the evolution of infrared dark hubs: JVLA observations of SDC13

G. M. Williams[1], N. Peretto[1], A. Avison[2,3], A. Duarte-Cabral[1], and G. A. Fuller[2]

背景：フィラメントが集中している箇所（hub）は、星団・大質量星形成と深い関わり。
　　ハブの進化とそこでの星形成の関係の理解は重要。

目的：SDC13の運動・密度構造を調べ、進化やfragmentationの駆動源を決める

観測：NH_3(1,1) & NH_3(2,2) 輝線 with Jansky Very Large Array, Green Bank Telescope (0.07 pc)

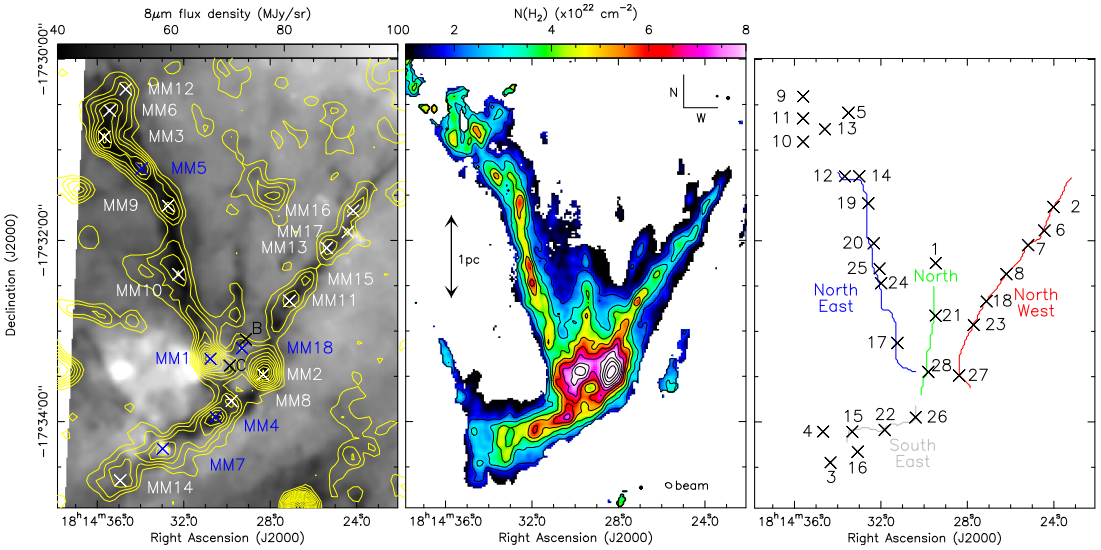

Fig. 5. *Left*: Spitzer 8 μm flux density in units of MJy/sr, overlaid with IRAM 30m MAMBO 1.2mm dust continuum contours in steps of 5mJy/beam, from 3mJy/beam to 88mJy/beam. Crosses denote the positions of identified 1.2mm MAMBO compact sources (white for starless and blue for protostellar, Peretto et al. 2014) and two 1.3mm SMA continuum sources (in black crosses, McGuire et al. 2016). *Middle*: H_2 column density map in units of 10^{22} cm^{-2}, derived from the NH_3 integrated intensity. Overlaid contours are placed in 1×10^{22} cm^{-2} steps, from 2×10^{22} cm^{-2} to 12×10^{22} cm^{-2}. *Right*: Plot showing the extracted cores (black crosses, numbered according to Table 2) and filaments (labelled coloured lines). The extraction of these structures are discussed in Section 4. Extra cores at the outskirts of the North-East and South-East arms are in the more diffuse regions of the cloud where the spines did not extend through. Spine colours match those in subsequent figures.

全ての hubフィラメントはsupercritical
（transonicの非熱的な速度分散を持つ）

　コアの間隔：　フィラメントに沿って~0.37pc

フィラメントの年齢：a few Myer（非平衡フィラメントの半解析的モデル（Clarke+16, 17）を使用）

　<= Peretto+14の力学的タイムスケールとconsistent

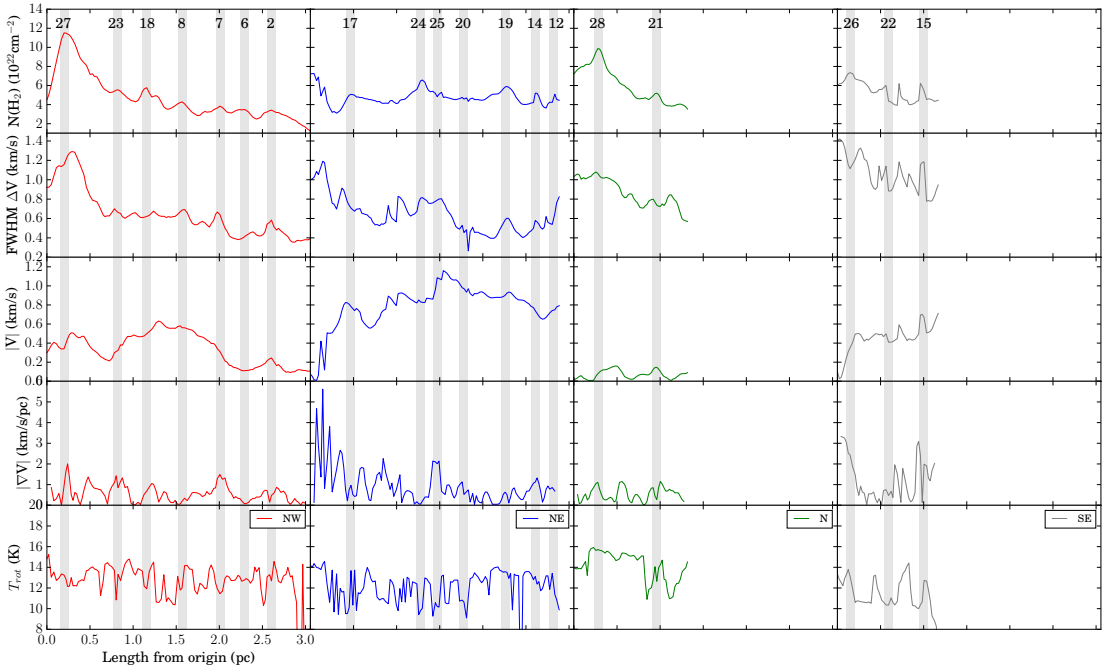

Fig. 8. Profiles along the spines, where each column denotes a different filament (North-West in red, North-East in blue, North in green and South-East in grey). The origin of each spine was centred at the hub region. The first row plots the column density of H_2 calculated from the fitted NH_3 integrated intensity. The second row plots the FWHM velocity width, while the third row plots the absolute centroid line-of-sight velocity (offset from the cloud systemic velocity of 37 km s^{-1}), both also from the hyperfine structure fitting. The fourth row plots the absolute velocity gradient evaluated over the mean core size of ~0.1 pc. The fifth row plots the rotational temperature derived from the NH_3 emission (see Appendix B.2) which has a standard deviation of 1.8 K. The drops of temperature below 8 K are artificial and due to missing NH_3(2,2) detections at these particular locations. The vertical shaded regions in each panel correspond to the peak $N(H_2)$ positions of the cores along the spine, and are ~0.1 pc wide.

・2つのフィラメントでの大きな視線速度勾配：
　重力に起因するものではなく、HII領域からの圧縮の可能性が高い

・同定コアの73%で速度分散が増加：
　フィラメントの分裂過程に起因する物質の蓄積の結果と解釈

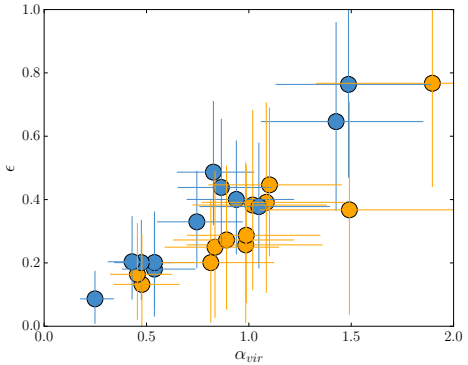

Fig. 19. Observed virial ratio plotted against the energy conversion efficiency of gravitational energy into kinetic energy for the combined JVLA/GBT data (in blue), and the JVLA–only data (in orange). Only starless along the filaments are plotted, as protostellar or hub centre cores are subject to extra energy source that will effect the estimate of ϵ. Errors were propagated using a Monte Carlo error propagation method.

コアでの重力エネルギーから運動エネルギーへ変換効率を求めた（$\varepsilon \sim 35$ %）
<= 理論値よりも大きい

フィラメントの結合部に最もmassiveなコアが付随
（速度分散は最も大きい）
　<= ハブ形状によって生まれる加速度勾配に起因すると考えられる

SDC13の進化シナリオ：
超音速乱流でのpost shock構造として、フィラメントが形成
乱流エネルギーの散逸の結果、高密度コアは亜音速に
重力が優位になり、hubの進化を促す。
　　それによって、重力エネルギーは運動エネルギーへと変換される
フィラメント連結部でのより大きな重力加速度勾配の発生が、大質量コア形成を促進

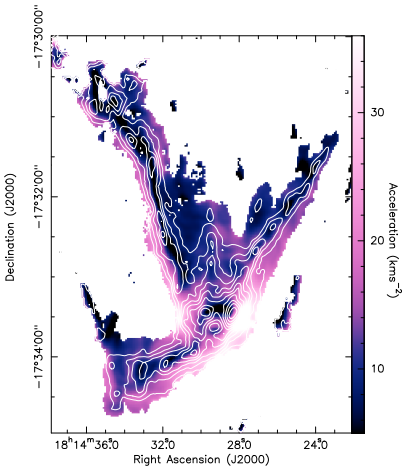

Fig. 20. Map of gravitational acceleration in SDC13 in units of 1×10^{-12} km s^{-2}. Mass was calculated from the H_2 column density map in the middle panel of Figure 5. Contours are of the H_2 column density in Figure 5, plotted in 1×10^{22} cm^{-2} steps, from 2×10^{22} cm^{-2} to 12×10^{22} cm^{-2}.